INSTITUTE OF PHYSICS PUBLISHING SEMICONDUCTOR SCIENCE AND TECHNOLOGY

Semicond. Sci. Technol. **20** (2005) 886–893 doi:10.1088/0268-1242/20/8/046

Below bandgap optical absorption in tellurium-doped GaSb

A Chandola, R Pino and P S Dutta

Department of Electrical, Computer and Systems Engineering,
Rensselaer Polytechnic Institute, Troy, NY 12180, USA

E-mail: duttap@rpi.edu

Received 9 May 2005, in final form 14 June 2005
Published 18 July 2005
Online at stacks.iop.org/SST/20/886

Abstract

Enhancement in below bandgap room temperature infrared transmission has been observed in tellurium (Te)-doped GaSb bulk crystals. The effect of Te concentration on the transmission characteristics of GaSb has been experimentally and theoretically analysed. Undoped GaSb is known to exhibit p-type conductivity with residual hole concentration of the order of (1–2) $\times$ 10^{17} cm^{-3} at room temperature due to the formation of native defects. For such samples, inter-valence band absorption has been found to be the dominant absorption mechanism. The residual holes could be compensated by n-type dopants such as Te. With increasing Te concentration, free carrier absorption due to electrons and inter-valley transitions in the conduction subband become significant. The dependences of various absorption mechanisms as a function of wavelength have been discussed in this paper.

1. Introduction

Gallium antimonide (GaSb) is a technologically important III–V semiconductor substrate material because its lattice parameter matches solid solutions of various ternary and quaternary III–V compounds whose bandgaps cover a wide spectral range from 0.3 to 1.58 eV (0.8–4.3 μm) [1, 2]. GaSb-based device structures have shown potential for applications in laser diodes with low threshold voltage [3, 4], photodetectors with high quantum efficiency [5, 6], high-frequency devices [7, 8], superlattices with tailored optical and transport characteristics [9], booster cells in tandem solar cell arrangements for improved efficiency of photovoltaic cells [10] and high-efficiency thermophotovoltaic (TPV) cells [11]. Also, detection of longer wavelengths, 8 to 14 μm, is possible with inter-subband absorption in antimonide-based superlattices [12].

One of the main limitations with the antimonide technology is the unavailability of semi-insulating (high resistivity) or optically transparent GaSb substrates demonstrating low absorption coefficients. Commercially available substrates show high infrared absorption ($\alpha \approx 100$ cm^{-1}) in the below bandgap regime. It is desirable to have the absorption coefficient as low as possible. As-grown undoped GaSb is always p-type in nature irrespective of growth technique and conditions. These residual acceptors are the limiting factors for both fundamental studies and device applications [1]. The residual acceptors with concentration of 10^{17} cm^{-3} have been found to be related to gallium vacancies (V_{Ga}) and to gallium antisites (Ga_{Sb}) with a doubly ionizable nature [13]. Efforts to reduce these native acceptors such as growth at low temperatures (from solutions and vapour phase) as well as from non-stoichiometric melts had limited success [1]. Specific efforts that led to improvement in the optical transparency in the crystals include lithium diffusion in undoped p-GaSb by Hrostrowski and Fuller [14] and tellurium compensation by Milvidskaya *et al* [15]. The latter study only reported resistivity and transmission of GaSb at 77 K. To the best of our knowledge, a thorough systematic study of the optical properties of Te-doped GaSb at room temperature has not been reported in the literature. We have been able to enhance the transmission (reduce absorption) by impurity compensation. This paper focuses on the analysis of the optical absorption mechanisms in GaSb with the goal of identifying carrier concentration that could lead to high transparency substrates.

Table 1. Electrical characteristics obtained from Hall measurements at 300 K for different wafers.

Sample name	Type	Concentration (cm^{-3})	Mobility ($cm^2\ V^{-1}\ s^{-1}$)
W_0	p	5.3×10^{16}	782
W_1	p	3.2×10^{16}	442
W_6	p	1.4×10^{16}	72
W_7	n	2.3×10^{16}	783
W_{10}	n	8.9×10^{16}	1355
W_{11}	n	1.3×10^{17}	3548
W_{12}	n	2.2×10^{17}	2592
W_{16}	n	1.3×10^{18}	1282

2. Experimental observations

The GaSb bulk crystal (50 mm diameter) was grown using the vertical Bridgman technique [16]. Considering the fact that undoped GaSb has (1–2) $\times\ 10^{17}$ cm^{-3} acceptors and the segregation coefficient of Te in GaSb to be 0.37 [17], the initial Te concentration in the melt was set at 1×10^{18} cm^{-3} in order to obtain the highest level of compensation at approximately midway along the growth axis of the boule. After growth, the crystal was sliced into wafers and polished on both sides using commercial alumina-based slurries [16]. W_0 is the wafer sliced from the first to freeze section of the boule with the lowest Te concentration. The samples indices (W_1, W_2, W_3, etc) denote the position of the wafer sliced along the growth axis starting from W_0. The optical and electrical characterizations were performed using a NEXUS 670 Fourier transform infrared (FTIR) spectrometer (from Thermo Nicolet) and an EGK HEM-2000 Hall measurement system, respectively, at 300 K. Table 1 gives the nomenclature and electrical characteristics of the samples [16]. In this paper, we will discuss only the optical characteristics of the samples while correlating them with the electrical properties (presented in table 1).

Assuming multiple reflections inside the sample (as $\alpha t < 1$ for our measured samples) and the absence of fringes, transmission spectra can be converted to absorption spectra by applying the following relation,

$$T = \frac{(1-R)^2\,\mathrm{e}^{-\alpha t}}{1-R^2\,\mathrm{e}^{-2\alpha t}}, \tag{1}$$

where α is the absorption coefficient and t is the thickness of the sample. Reflectivity, R, is calculated with the assumption that the refractive index, n, remains constant for the entire wavelength range under consideration i.e. $\lambda < 20\ \mu$m. Under this assumption, R, for a normally incident beam, is given by

$$R = \left(\frac{n-1}{n+1}\right)^2 \tag{2}$$

where for GaSb, the refractive index is taken as 3.8 [18]. With these formulations α can be calculated at all wavelengths from the experimentally obtained transmission spectra of the various samples.

3. Optical absorption analyses

Very limited studies have been reported on the infrared absorption in GaSb [19–22] compared to other III–V and elemental semiconductors. Optical absorption mechanisms in semiconductors have been discussed by Pankove [23]. Depending on the material, temperature and the wavelength range of interest, various absorption mechanisms dominate to different degrees. The optical absorption mechanisms of interest for below bandgap absorption at room temperature are as follows:

(1) free carrier absorption (FCA) by free electrons;
(2) free carrier absorption by free holes;
(3) inter-valence band absorption by holes;
(4) inter-valley conduction band absorption by electrons.

Depending on the relative concentration of the electrons and holes, one or more mechanisms can be effective for a given doping concentration in the sample.

3.1. Free carrier absorption

Scattering of free carriers leads to the absorption of the incident radiation. Free carrier absorption by free electrons has classically been modelled by the Drude-Zener theory which yields

$$\alpha_{\mathrm{FCA}} = \left(\frac{e^3}{4\pi^2 c^3 m_0^2 \epsilon_0}\right)\left(\frac{1}{n(m^*/m_0)^2}\right)\left(\frac{\lambda^2}{\mu}\right)N = s\lambda^2 N \tag{3}$$

where α_{FCA} is the free carrier absorption coefficient, n is the refractive index, m^* is the effective mass of the carrier, μ is the mobility, N is the carrier concentration and λ is the incident wavelength. However, application of quantum mechanical principles yields different values for the exponent of the wavelength. The exponents depend on the dominant scattering mechanism. The collision with the semiconductor lattice results in scattering by acoustic phonons which leads to an absorption increase as $\lambda^{1.5}$ [24]. Scattering due to optical phonons gives a dependence of $\lambda^{2.5}$ [25], while scattering by ionized impurities gives a dependence of λ^3 or $\lambda^{3.5}$, depending on the approximations used in the theory [26]. According to [23], in general all three modes of scattering are present. Thus the overall absorption coefficient for electrons due to free carrier absorption is given by a weighted sum of the different processes

$$\alpha_{\mathrm{FCA}} = s(A\lambda^{1.5} + B\lambda^{2.5} + C\lambda^3) \tag{4}$$

where s is a constant as defined in equation (3). A, B and C are the fitting parameters.

To reduce the number of fitting parameters, one can fit the free carrier absorption data to the following equation,

$$\alpha_{\mathrm{FCA}} = K_{\mathrm{FCA}}\lambda^m, \tag{5}$$

where K_{FCA} is a proportionality constant dependent on doping. This constant also takes into account any dependence of mobility on doping (compare equations (3) and (5)). With this approach we will have only two parameters, namely m and K_{FCA}, which are easier to deduce than deriving three independent parameters.

A similar formulation can be made to represent the free carrier absorption due to holes.

3.2. Inter-valence band absorption

Valence band structure in III–V compounds is explained by the traditional Kane model [27]. The three bands constituting the valence band are called the heavy hole (hh), the light hole (lh) and the split-off (so) bands. Transitions of carriers within these bands are allowed and this gives rise to the inter-valence band absorption.

Kahn has treated these transitions for a three band Kane model [28]. Absorption coefficients resulting from transitions between different bands in the valence band are given by

$$\alpha_{\mathrm{lh-hh}} = \frac{1}{4\pi\epsilon} \times \frac{16\pi^2\sqrt{2}e^2\hbar^{3/2}A_{\mathrm{VB1}}^2 m_{\mathrm{hh}}^* m_{\mathrm{lh}}^{*5/2} N\nu^{1/2}}{nc[1+(m_{\mathrm{lh}}/m_{\mathrm{hh}})^{3/2}]m_0^2(m_{\mathrm{hh}}^*-m_{\mathrm{lh}}^*)^{5/2}(kT)^{3/2}} \times \left[\exp\left(-\frac{h\nu}{kT}\frac{m_{\mathrm{lh}}^*}{m_{\mathrm{hh}}^*-m_{\mathrm{lh}}^*}\right) - \exp\left(-\frac{h\nu}{kT}\frac{m_{\mathrm{hh}}^*}{m_{\mathrm{hh}}^*-m_{\mathrm{lh}}^*}\right)\right], \quad (\nu > 0) \tag{6}$$

$$\alpha_{\mathrm{so-hh}} = \frac{1}{4\pi\epsilon} \times \frac{16\pi^2\sqrt{2}e^2\hbar^{3/2}A_{\mathrm{VB2}}^2 m_{\mathrm{hh}}^* m_{\mathrm{so}}^{*5/2} N(\nu-\nu_0)^{3/2}}{nc[1+(m_{\mathrm{lh}}/m_{\mathrm{hh}})^{3/2}]m_0^2(m_{\mathrm{hh}}^*-m_{\mathrm{so}}^*)^{5/2}\nu(kT)^{3/2}} \times \left[\exp\left(-\frac{h(\nu-\nu_0)}{kT}\frac{m_{\mathrm{so}}^*}{m_{\mathrm{hh}}^*-m_{\mathrm{so}}^*}\right)\right], \quad (\nu > \nu_0) \tag{7}$$

$$\alpha_{\mathrm{so-lh}} = \frac{1}{4\pi\epsilon} \times \frac{16\pi^2\sqrt{2}e^2\hbar^{3/2}A_{\mathrm{VB3}}^2 (m_{\mathrm{lh}}/m_{\mathrm{hh}})^{3/2} m_{\mathrm{lh}}^* m_{\mathrm{so}}^{*5/2} N(\nu_0-\nu)^{3/2}}{nc[1+(m_{\mathrm{lh}}/m_{\mathrm{hh}})^{3/2}]m_0^2(m_{\mathrm{so}}^*-m_{\mathrm{lh}}^*)^{5/2}\nu(kT)^{3/2}} \times \left[\exp\left(-\frac{h(\nu_0-\nu)}{kT}\frac{m_{\mathrm{so}}^*}{m_{\mathrm{so}}^*-m_{\mathrm{lh}}^*}\right)\right], \quad (\nu < \nu_0) \tag{8}$$

where ν is the frequency of incident radiation, n is the refractive index, ϵ is the permittivity, m_{lh}^*, m_{hh}^* and m_{so}^* are the effective masses of light holes, heavy holes and split-off holes respectively, m_0 is the electron rest mass and $A_{\mathrm{VB}i}$ is a dimensionless parameter. The $A_{\mathrm{VB}i}^2\hbar^2k^2$ is the square of the matrix element averaged over all directions for the different bands. $A_{\mathrm{VB}i}$ is treated as a fitting parameter. Also, there has been a large discrepancy in the reported values of effective masses of holes in III–V compounds ([29] and references therein). This is due to the complexity in the valence band structures. In the light of this discussion, we treat effective masses in the expression for inter-valence band absorption as fitting parameters. The parameter ν_0 is related to the energy of split-off band at $\mathbf{k} = 0$ and can be expressed as $E_{\mathrm{so}} = h\nu_0$. For GaSb, E_{so} is ascertained to be 0.8 eV [18]. Since the bandgap of GaSb is only 0.73 eV, direct transitions from split-off band to heavy hole band are not possible for below bandgap radiation. So $\alpha_{\mathrm{so-hh}}$ is not considered for below bandgap absorption. Another effect of E_{so} being larger than the incident radiation is that the term $(\nu_0 - \nu) \gg \nu$ in $\alpha_{\mathrm{so-lh}}$. Comparing the terms $\exp(-(\nu_0 - \nu))$ to $\exp(-\nu)$, we can easily determine that $\alpha_{\mathrm{lh-hh}} \gg \alpha_{\mathrm{so-lh}}$. Thus the inter-valence band absorption is mainly due to the transitions from the light hole to heavy hole band in GaSb. Hence, for the below bandgap regime the absorption coefficient for inter-valence band absorption, α_{IVB}, can be approximated by $\alpha_{\mathrm{lh-hh}}$.

3.3. Inter-valley conduction band electron absorption

Indirect electron transitions between minima at different k of the same conduction subband have been demonstrated in many III–V compound semiconductors. Spitzer and Whelan point out that for wavelengths near the intrinsic band edge, this absorption is proportional to the carrier concentration in n-GaAs [30]. Similar transitions have been observed in n-GaSb [31] and n-InP [32]. Lorenz *et al* [32] give the following expression for the dependence of this absorption on wavelength,

$$\alpha \propto (\hbar\omega - E_0)^{1/2}, \tag{9}$$

where E_0 is the threshold energy for such transitions to occur. The expression for E_0 is given by [23]

$$E_0 = \Delta E + E_{\mathrm{p}} - \xi_{\mathrm{n}} \tag{10}$$

which includes ΔE, the energy separation between the valleys, E_{p}, the phonon energy involved in the transition and ξ_{n}, the position of the Fermi level.

Rewriting equation (9) in terms of wavelengths, we can express the absorption due to transitions to different valleys in the same conduction subband as

$$\alpha_{\mathrm{CB}} = K_{\mathrm{CBV}}\left(\frac{1.24}{\lambda} - E_0\right)^{1/2} \tag{11}$$

where λ is the incident wavelength, and K_{CBV} and E_0 are the fitting parameters and they depend on the carrier concentration. This absorption is only possible if the energy separation between the valleys in the conduction band is comparable to the incident radiation. This absorption coefficient decreases with the increase in wavelength [32].

3.4. Below bandgap optical absorption coefficient

Thus the overall absorption coefficient can now be given by

$$\alpha = \alpha_{\mathrm{FCA_e}} + \alpha_{\mathrm{FCA_h}} + \alpha_{\mathrm{IVB}} + \alpha_{\mathrm{CB}}. \tag{12}$$

We see that for a p-type sample, where $p \gg n_{\mathrm{i}}$ (where n_{i} is the intrinsic carrier concentration), the major contribution to absorption comes from the inter-valence band and free hole absorption. For an intrinsic or near intrinsic sample, both the electron and hole contributions play an important role. For an n-type sample, where $n \gg n_{\mathrm{i}}$, major contribution comes from inter-valley conduction band and free electron absorption mechanisms. Thus depending on the carrier concentration, the below bandgap optical absorption characteristics in GaSb change considerably.

4. Results and discussion

Figures 1 and 2 show the transmission and absorption spectra of p-type and n-type GaSb samples, respectively doped with various degrees of tellurium. The transmission spectra for p-type samples exhibit an interesting shape as shown in figure 1. At the intrinsic band edge the transmission attains a maximum and starts decreasing rapidly for increasing wavelengths. However, this decrease in transmission saturates after a given wavelength and the transmission remains constant for higher wavelengths. The magnitude of this final saturated transmission value seems to vary with Te doping concentration. For the n-type samples, the transmission

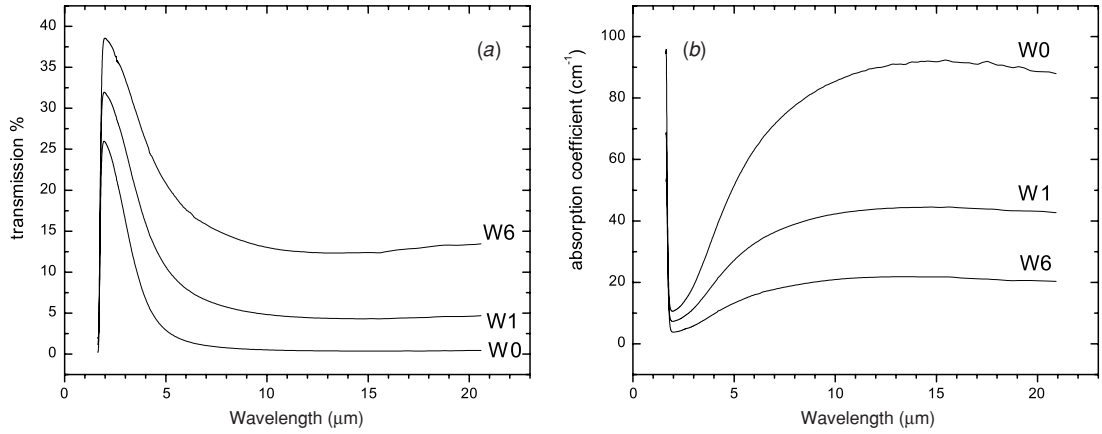

Figure 1. (*a*) FTIR transmission spectra and (*b*) calculated absorption spectra for the heavily compensated p-type Te-doped GaSb samples, namely W_0 ($t = 0.52$ mm), W_1 ($t = 0.52$ mm) and W_6 ($t = 0.58$ mm).

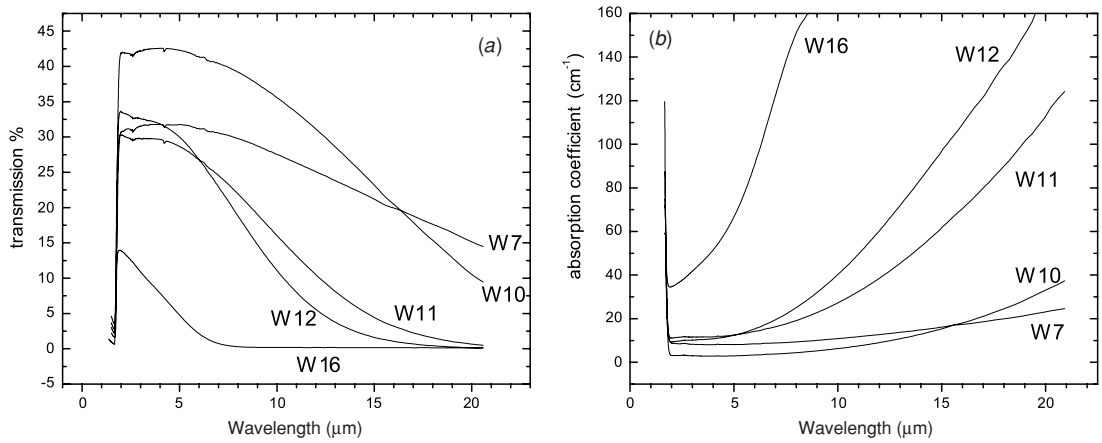

Figure 2. (*a*) FTIR transmission spectra and (*a*) calculated absorption spectra for the n-type Te-doped GaSb samples, namely W_7 ($t = 0.46$ mm), W_{10} ($t = 0.43$ mm), W_{11} ($t = 0.37$ mm), W_{12} ($t = 0.34$ mm) and W_{16} ($t = 0.33$ mm).

spectra (figure 2) shows a different shape. At the intrinsic band edge the transmission rises up to a maximum. For lowly doped samples it is seen that the transmission remains constant till it reaches a wavelength after which a rapid decrease in transmission is observed. Unlike the p-type samples this decrease does not saturate at longer wavelengths. The characteristic wavelength after which the transmission drops rapidly appears to be a function of extrinsic doping. For sample W_{10} this characteristic wavelength seems to be $\approx$6.5 μm while for sample W_{16} which is heavily Te doped the characteristic wavelength seems to coincide with the intrinsic band edge. Hence, in principle one could achieve a very broad transmission range in GaSb by fine tuning the compensation ratio. Theoretically highest transmission possible for below bandgap regime in GaSb is $\approx$49%, which is obtained by substituting $\alpha = 0$ in equation (1).

As discussed in section 3, the theoretical analysis of the experimental transmission involves a number of fitting parameters. However depending on the relative concentration of electrons and holes, only a few of these parameters play an effective role. For example, for a p-type sample such as W_0, the effective parameters are those which are related to the absorption due to holes, namely $A_{\mathrm{VB1}}, m^*_{\mathrm{lh}}, m^*_{\mathrm{hh}}$ and the free hole absorption parameters (equations (6) and (4)). Other parameters that describe the absorption due to electrons are not important for this sample. This is because the number of electrons is so low, that physically their contribution to optical absorption is negligible. Similarly for the n-type samples, since the hole concentrations are so low, the effective parameters are K_{FCA} and m (equation (5)) for free electron absorption and K_{CBV} and E_0 (equation (11)) for the inter-valley conduction band absorption. Tables 2 and 3 present these fitting parameters for our samples.

Table 2. Fitting parameters for inter-valence band absorption for various p-type samples.

Sample name	Concentration (cm^{-3})	Fitting parameters for inter-valence band absorption		
		m^*_{lh}	m^*_{hh}	A_{VB1}
W_0	5.3×10^{16}	0.05	0.33	33.69
W_1	3.2×10^{16}	0.05	0.33	31.61
W_6	1.4×10^{16}	0.05	0.33	32.55

For the p-type samples, contribution to the absorption coefficient arises from inter-valence band absorption (IVB) and hole free carrier absorption ($\mathrm{FCA_h}$). Since $\mathrm{FCA_h}$ is expected to contribute significantly only for the longer wavelengths, on account of the λ^m dependence, the dominant absorption mechanism for shorter wavelengths near the band

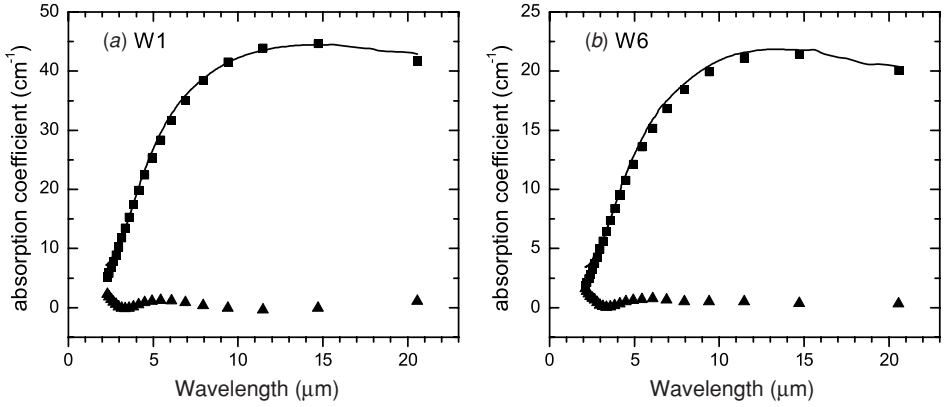

Figure 3. Contribution of inter-valence band (IVB) absorption (■) and the hole free carrier absorption (FCA) (▲) to the total optical absorption (solid line) for wafers W_1 and W_6 (p-type GaSb). Note that the free hole absorption is negligible when compared to the IVB contribution. Similar curves are obtained for other p-type wafers too.

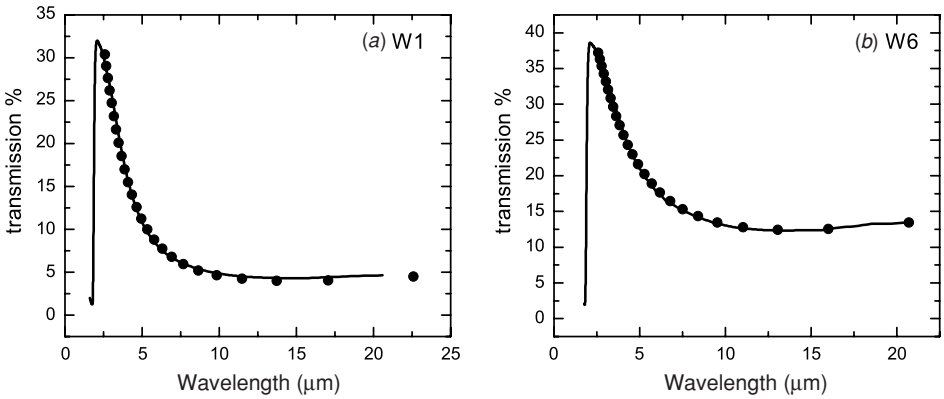

Figure 4. Theoretically fitted curves (•) to experimental data (solid line) for wafers W_1 and W_6.

Table 3. Fitting parameters for electron free carrier absorption and inter-valley conduction band absorption mechanisms in n-type samples (constants valid for units of wavelengths in μm and energies in eV).

Sample name	Concentration (cm^{-3})	Mobility ($cm^2\ V^{-1}\ s^{-1}$)	Free carrier absorption parameters		Inter-valley conduction band absorption parameters		
			K_{FCA}	m	K_{CBV}	E_0	C
W_{16}	1.3×10^{18}	1282	3.190	1.87	43.95	0.240	−3.0
W_{12}	2.2×10^{17}	2592	0.302	2.13	16.12	0.167	−1.3
W_{11}	1.3×10^{17}	3548	0.203	2.11	17.15	0.108	−0.2
W_{10}	8.9×10^{16}	1355	0.013	2.62	4.83	0.090	0.0
W_7	2.3×10^{16}	783	0.635	1.19	12.38	0.085	−1.3

edge is expected to be IVB. Hence, the wavelength range between 2.5 μm and 5 μm is chosen to fit experimental data to theory for the IVB mechanism and the fitting parameters for IVB are derived. The fitting parameters so obtained are tabulated in table 2. Excellent fits could be obtained for all the samples with the values shown in the table. The absorption curve was then extrapolated for longer wavelengths using these values to determine the contribution of the IVB mechanism. This was then subtracted from the total absorption curve to obtain the FCA_h contribution. Contributions to hole absorption from these two mechanisms, for wafers W_1 and W_6 are shown in figure 3. The figure shows absorption spectra typical of a p-type wafer. Note that for these samples, hole free carrier absorption is negligible. Similarly for all the other samples, contribution from hole FCA was less than 9% of the total absorption coefficient. Due to this small contribution of FCA_h, any fitting parameter is bound to have large errors associated with it. Hence, in our analysis we choose to neglect the effects of hole free carrier absorption. Figure 4 shows the theoretically fitted transmission plots overlaid on experimental data for wafers W_1 and W_6. Note the excellent fit of theory to experimental data. W_1 and W_6 differ only in the magnitude of the hole concentration. Lesser hole concentration in W_6 is due to increased Te content, which compensates the native defects. It is clear that with increasing Te content, residual hole concentration decreases resulting in enhancement in the transmission.

For the n-type Te-doped GaSb samples the dominant absorption mechanisms are inter-valley conduction band (CBV) absorption and the electron free carrier absorption

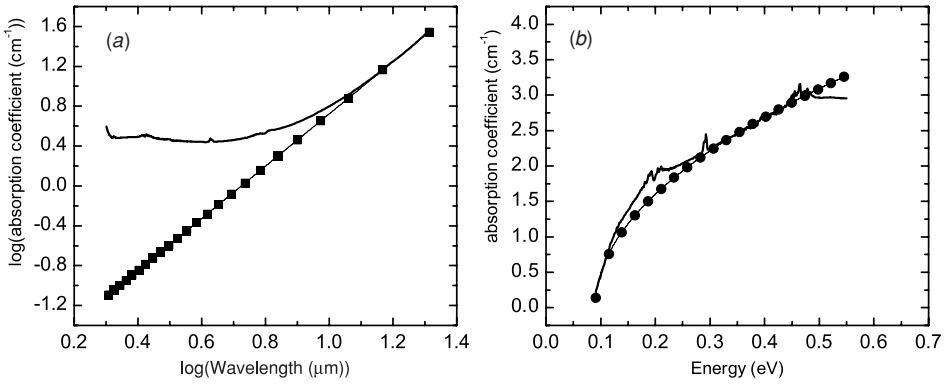

Figure 5. Typical steps for theoretical fitting to experimental data for n-type GaSb sample (wafer W_{10}). (*a*) Fitting FCA equation (■) for longer wavelengths where CBV absorption does not occur to the total experimental absorption spectra (solid line), (*b*) CBV absorption (solid line) is obtained by subtracting extrapolated FCA contribution from the experimental absorption spectrum. This is fitted to the inter-valley conduction band absorption equation (●).

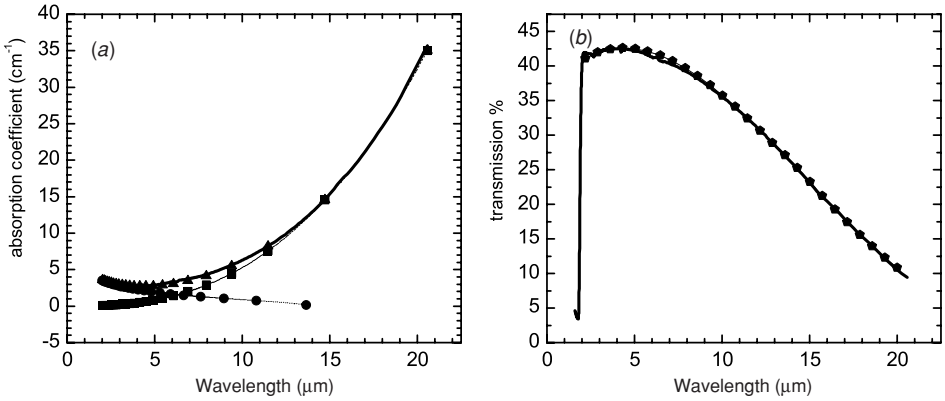

Figure 6. For wafer W_{10} (*a*) contribution from different absorption mechanisms, CBV (●), FCA (■) and their sum (▲) is shown along with experimental data (solid line). (*b*) Transmission curves from the fitted parameters (♦) plotted with experimental transmission spectrum (solid line).

(FCA_e). Equation (5) indicates that contribution from FCA_e increases with increasing wavelengths while CBV absorption, as given by equation (11), decreases with increasing wavelength. For wavelengths beyond $\lambda_0 = 1.24/E_0$ (λ_0 in μm and E_0 in eV from equation (11)), this mechanism does not contribute anymore. The closest valley above the Γ valley in GaSb is the L valley and the energy difference between them is 0.08 eV [18]. The corresponding wavelength of the radiation with this energy is 15.5 μm. Thus we can safely conclude that CBV absorption mechanism does not contribute beyond 15.5 μm and the sole contributor to absorption would be the FCA_e mechanism. We derive the FCA_e parameters, namely K_{FCA} and m, by fitting equation (5) to the experimental data between 15.5 and 20 μm. These parameters for different wafers are given in table 3. Figure 5(*a*) shows the extraction of FCA_e parameters from a log–log plot for absorption coefficient against wavelength. The contribution of FCA_e mechanism is then extrapolated for shorter wavelengths and subtracted from the total experimental absorption spectrum to obtain the contribution due to the CB absorption mechanism. This remainder is then fitted to equation (11) to derive the CB fitting parameters, namely K_{CBV} and E_0. This step is represented in figure 5(*b*). Equation (11) is modified to

$$\alpha_{CB} = K_{CBV}\left(\frac{1.24}{\lambda} - E_0\right) + C. \qquad (13)$$

The constant, C, is added to the equation to take into account any contribution of FCA_e to α_{CBV}. Since we extrapolate the contribution of FCA_e for shorter wavelengths, there is always either overestimation or underestimation involved in the procedure. This might affect the fitting for CBV absorption mechanism. The constant is a result of such extrapolation errors. These parameters are also tabulated in table 3. Figure 6(*a*) shows the contribution from the two absorption mechanisms. Note that as expected, the contribution of FCA_e increases with wavelength while CBV absorption decreases with wavelength. These opposite trends lead to the observed constant transmission for wavelengths closer to the band edge. The figure also shows the total absorption mechanism calculated from the equations using the fitting parameters derived in table 3. An excellent fit with the experimentally obtained absorption spectrum is observed. The theoretically fitted absorption spectrum is converted to the transmission spectrum and is shown in figure 6(*b*) along with the actual experimental transmission spectrum.

As the electron concentration increases from $4.2 \times 10^{16}\,cm^{-3}$ to $1.3 \times 10^{18}\,cm^{-3}$, the value for E_0 keeps increasing from 0.09 eV to 0.3 eV (refer to table 3). Interestingly, 0.3 eV is the separation between the Γ and X valleys [18]. This suggests that with increasing electron concentration, transitions are possible between Γ and X as well as Γ and

L valleys. Additionally, the increase in carrier concentration increases the contribution of FCA_e mechanism towards the total absorption coefficient. This contribution is strong enough so as to mask out any effects of transitions from the Γ to L valley which might result in a higher value for the fitting parameter E_0.

The exponent of the wavelength variation in the FCA_e mechanism is related to the dominant scattering mechanism as explained in the section on theory of free carrier absorption. The exponents for various samples are listed in table 3. The proportionality constant, K_{FCA}, is dependent in a complex manner upon doping (compare equations (3) and (5)). This is because electron mobility variation with impurity concentration for n-GaSb is very different from other III–V compounds. As seen in table 3, the mobility increases with increasing Te content and then decreases again for very high concentrations. This is accounted by the additional screening of the electrons as the higher lying conduction band valley gets filled up. However, after a certain concentration, electron–electron scattering comes into effect and as a result the mobility reduces [33]. Thus it should be noted that the variation of K_{FCA} is not a simple dependence on doping. However, it seems to follow the same trend as the mobility variation with doping (refer to table 3). This makes the optical capture cross-section in n-GaSb, a function of doping for longer wavelengths.

From the theory presented above, it is clear that electron concentration plays an important role in determining the transmission characteristics. As the electron concentration increases, theory predicts an increase in the optical absorption (samples W_{10} through W_{16}). Additionally, mobility also plays an important role in free carrier absorption. With increasing impurity concentration (samples W_7 through W_{10}) the electron mobility increases resulting in a decrease in the optical absorption although the electron concentration increases. From this discussion it can be deduced that due to the inverse dependence of optical absorption on electron concentration and mobility (refer to equation (3)) and the peculiar dependence of mobility on electron concentration, the optical absorption decreases as the impurity concentration is increased from low to moderate values and then increases as the impurity concentration is increased further. Thus it can be said that for a particular impurity concentration, the trade-off between electron concentration and mobility will be such that the optical transmission will reach a maximum. From table 3, for GaSb grown from stoichiometric melts, the Te impurity concentration required for maximum transmission is such that will give rise to an electron concentration between $5 \times 10^{16}\,cm^{-3}$ and $1 \times 10^{17}\,cm^{-3}$. Another way to enhance the transmission is to reduce the number of compensating native defect centres. A simple way of reducing the native defect concentration is to grow n-GaSb from non-stoichiometric melts. If the native defect concentration is reduced then for the same Te concentration enhanced electron mobilities are observed [33]. This provides us with low electron concentrations as well as high mobilities, which is required to further enhance transmission.

5. Conclusions

In conclusion, we presented the results of below bandgap absorption studies in heavily compensated p-type and n-type GaSb as a function of Te doping. For the p-type samples the transmission starts decreasing rapidly for wavelengths below the band edge and then saturates for longer wavelengths at a certain transmission value. As the Te doping level increases, the residual hole concentration reduces and an enhancement in transmission is observed. The optical absorption in p-type samples has been found to be dominated by the inter-valence band absorption mechanism. For the n-type samples, the transmission is constant for a certain range of wavelengths below the band edge, after which the transmission starts decreasing rapidly. The constant wavelength range reduces as the Te concentration increases. The magnitude of transmission increases with increasing electron concentration till $n \approx 8 \times 10^{16}\,cm^{-3}$, beyond which the maximum transmission value starts decreasing for increasing electron concentrations. These observations have been explained by taking into account free electron absorption and inter-conduction band valley absorption mechanisms along with the peculiar mobility dependence on doping concentration in GaSb.

Acknowledgment

This work was supported by the National Science Foundation (NSF) Faculty Early Career Development Award ECS 0093706.

References

[1] Dutta P S, Bhat H L and Kumar V 1997 *J. Appl. Phys.* **81** 5821
[2] Milnes A G and Polyakov A Y 1993 *Solid-State Electron.* **36** 803
[3] Motosugi G and Kagawa T 1980 *Japan. J. Appl. Phys.* **19** 2303
[4] Morosini M B Z, Herrera-Perez J L, Loural M S S, Von Zuben A A G, da Silveira A C F and Patel N B 1993 *IEEE J. Quantum Electron.* **29** 2103
[5] Hildebrand O, Kuebart W, Benz K W and Pilkuhn M H 1981 *IEEE J. Quantum Electron.* **17** 284
[6] Hildebrand O, Kuebart W and Pilkuhn M 1980 *Appl. Phys. Lett.* **37** 801
[7] Segawa K, Miki H, Otsubo M and Shirata K 1976 *Electron. Lett.* **12** 124
[8] Hilsum C and Rees H D 1970 *Electron. Lett.* **6** 277
[9] Esaki L 1981 *J. Cryst. Growth* **52** 227
[10] Frass L M, Girard G R, Avery J E, Arau B A, Sundaram V S, Thompson A G and Gee J M 1989 *J. Appl. Phys.* **66** 3866
[11] Williams D J and Fraas L M 1996 *Proc. 2nd NREL Conference on TPV Generation of Electricity (Colorado Springs, CO)* ed J P Benner, T J Coutts and D S Ginley (New York: AIP) p 134
[12] Xie H, Piao J, Katz J and Wang W I 1991 *J. Appl. Phys.* **70** 3152
[13] Baxter R D, Bate R T and Reid F J 1965 *J. Phys. Chem. Solids* **26** 41
[14] Hrostowski H J and Fuller C S 1958 *J. Phys. Chem. Solids* **4** 155
[15] Milvidskaya A G, Polyakov A Y, Kolchina G P, Milnes A G, Govorkov A V, Smirkov N B and Tunitskaya I V 1994 *Mater. Sci. Eng.* B **22** 279
[16] Pino R, Ko Y and Dutta P S 2004 *J. Appl. Phys.* **96** 1064
[17] Dutta P S and Ostrogorsky A G 1999 *J. Cryst. Growth* **197** 749
[18] Levinshtein M, Rumyantsev S and Shur M 1999 *Handbook Series on Semiconductor Parameters* vol 2 (Singapore: World Scientific) p 90
[19] Blunt R F, Hoseler W R and Frederikse H P R 1954 *Phys. Rev.* **96** 576
[20] Kaiser R and Fan H Y 1965 *Phys. Rev.* A **138** 156

[21] Iluridze G N, Titkov A N and Chalkina E I 1987 *Sov. Phys.—Semicond.* **21** 48
[22] Lavrushin B M, Nabiev R F and Popov Yu M 1988 *Sov. Phys.—Semicond.* **22** 441
[23] Pankove J I 1971 *Optical Processes in Semiconductors* (Engelwood Cliffs, NJ: Prentice-Hall)
[24] Fan H Y and Becker M 1951 *Semiconducting Materials* (London: Butterworth)
[25] Visvanathan S 1960 *Phys. Rev.* **120** 376
[26] Fan H Y, Spitzer W G and Collins R J 1956 *Phys. Rev.* **101** 566
[27] Kane E O 1956 *J. Phys. Chem. Solids* **1** 82
[28] Kahn A H 1955 *Phys. Rev.* **97** 1647
[29] Kolodziejczak J, Zukotynski S and Stramska H 1966 *Phys. Status Solidi* **14** 471
[30] Spitzer W G and Whelan J 1959 *Phys. Rev.* **114** 59
[31] Becker W M, Ramdas A M and Fan H Y 1961 *J. Appl. Phys.* **32** 2094
[32] Lorenz M R, Reuter W, Dumke W P, Chicotka R J, Pettit G D and Woodall J M 1968 *Appl. Phys. Lett.* **13** 421
[33] Baxter R D, Reid F J and Beer A C 1967 *Phys. Rev.* **162** 718